

**Catalysis Science & Technology**  
Electronic Supplementary Material (ESI) for Catalysis Science & Technology  
This journal is © The Royal Society of Chemistry 2014

## Electronic Supplementary Information (ESI)

Toward enhanced conversion of model biogas mixtures: Parametric tuning and mechanistic study for ceria-zirconia supported nickel-cobalt catalyst

Moom Sinn Aw,<sup>a</sup> Ilja Gasan Osojnik Črnivec<sup>a</sup> and Albin Pintar<sup>a,b</sup>

<sup>a</sup>Laboratory for Environmental Sciences and Engineering,  
National Institute of Chemistry, Hajdrihova 19,  
P. O. Box 660, SI-1001 Ljubljana, Slovenia

<sup>b</sup>Centre of Excellence “Low Carbon Technologies”, Hajdrihova 19, SI-1001 Ljubljana, Slovenia

\*To whom correspondence should be addressed. E-mail: moom.sinn.aw@ki.si  
Tel: +386(0)1/476 0249; Fax: +386(0)1/476 0460

## Experimental Methods

### S.1 Physicochemical characterization of CeZr/NiCo catalysts

**S.1.1 XRD analysis.** X-ray diffractograms were recorded on a PANalytical X'pert PRO monochromator-equipped diffractometer via CuK $\alpha$  radiation beam with a wavelength equal to 0.15406 nm. The powdered samples were scanned over 2 $\theta$  range of 5 to 90° with an increment of 0.034° and a measured time of 1 s for every increment at the angle.

**S.1.2 N<sub>2</sub> gas sorption.** N<sub>2</sub> physisorption was performed at -196 °C (Micromeritics, model Tristar II 3020) after samples were degassed in nitrogen flow for 1 h at 90 °C and then thermally heated for 4 h at 180 °C in the Micromeritics SmartPrep Degasser. Specific surface area was calculated by means of multipoint Brunauer-Emmett-Teller (BET) method, whereas pore volume and pore size distribution were determined using Barrett-Joyner-Halenda (BJH) method.

**S.1.3 He pycnometry.** High precision skeletal density of both fresh and spent catalyst samples was measured at constant ambient room temperature ( $25 \pm 2$  °C) with AccuPyc II 1340 microprocessor controlled gas pycnometer (Micromeritics), using a supply of high purity helium (He) for gas displacement within a standard 1 cm<sup>3</sup> specimen chamber under repeated purges with equilibrated pressure rate of 0.005 psig/min in a total of 10 measurement cycles.

**S.1.4 H<sub>2</sub>-TPR analysis.** Prior to H<sub>2</sub>-TPR measurements, all samples were weighed to ca. 15 mg before being mounted onto the platinum pan and loaded into the TG furnace. Each sample was degassed *in situ* under nitrogen flow at 50 NmL/min from RT to 300 °C, followed by isothermal heating for 1 h at 300 °C. Temperature was decreased to 50 °C and stabilized for 15 min after the pre-treatment. H<sub>2</sub>-TPR analysis was carried out with a gas flow of 4.5 vol. % H<sub>2</sub>/N<sub>2</sub> mixture at 115 NmL/min heated from 50 to 800 °C at a 5 °C/min heating ramp, followed by a 10 min isothermal step. Ideal plug flow was quasi-simulated by applying the conditions described by Monti and Baiker. Thus, the K parameter was calculated to check the quality of the H<sub>2</sub>-TPR and was found to be within acceptable value range.<sup>1</sup> The thermograms of weight versus temperature were plotted, mass normalized and their respective derivative mass curves were processed in Origin 8.1 software.

**S.1.5 FESEM examination.** Surface morphologies of the as-prepared supported catalysts, both fresh and spent, were characterized by FESEM (Oxford Instruments, model SUPRA 35 VP), whereby high resolution electron micrographs were generated using a FESEM SUPRA 35VP (Carl Zeiss) microscope.

**S.1.6 TG-DSC and TPO analysis.** All as-prepared fresh catalyst samples were weighed to ca. 15 mg and placed in a ceramic crucible before being loaded into the furnace of STA 6000 analyzer (Simultaneous Thermal Analyzer (STA) 6000, Perkin Elmer) to be heated until 800 °C at a scanning rate of 10 °C/min in 50 mL/min air. Likewise, the carbon content of carbonaceous deposits accumulated in the spent catalysts after MDR was also determined using the same instrument by means of TPO/TGA analysis. The extent of coking was thus determined by thermal decomposition of the samples using the same protocol. Furthermore, the TPO results were also ascertained using CHNS elemental analysis (2400 Series II Analyzer, Perkin Elmer), and the morphology of the spent catalyst was visualized through FESEM microscopic imaging.

## S.2 Results and discussion

### S.2.1 XRD diffractograms of CeZr mixed oxide solid solutions (support) and the supported catalysts

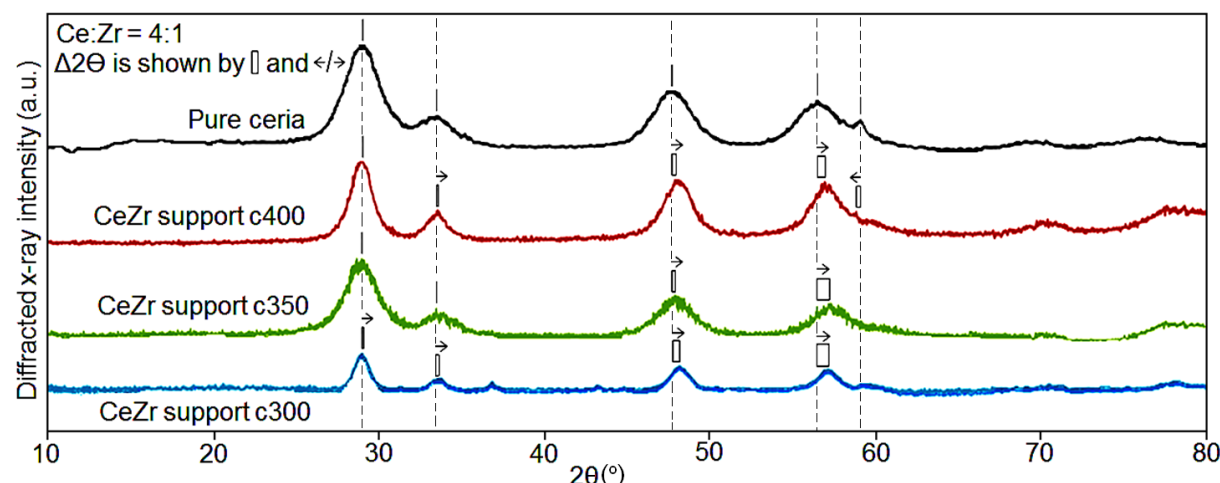


**Fig. S1** XRD diffractograms of CeZr mixed oxides support calcined at 300 °C, 350 °C and 400 °C, in comparison to pure ceria, with  $\Delta 2\theta$  displayed showing the shifting of the characteristics peaks from pure ceria.

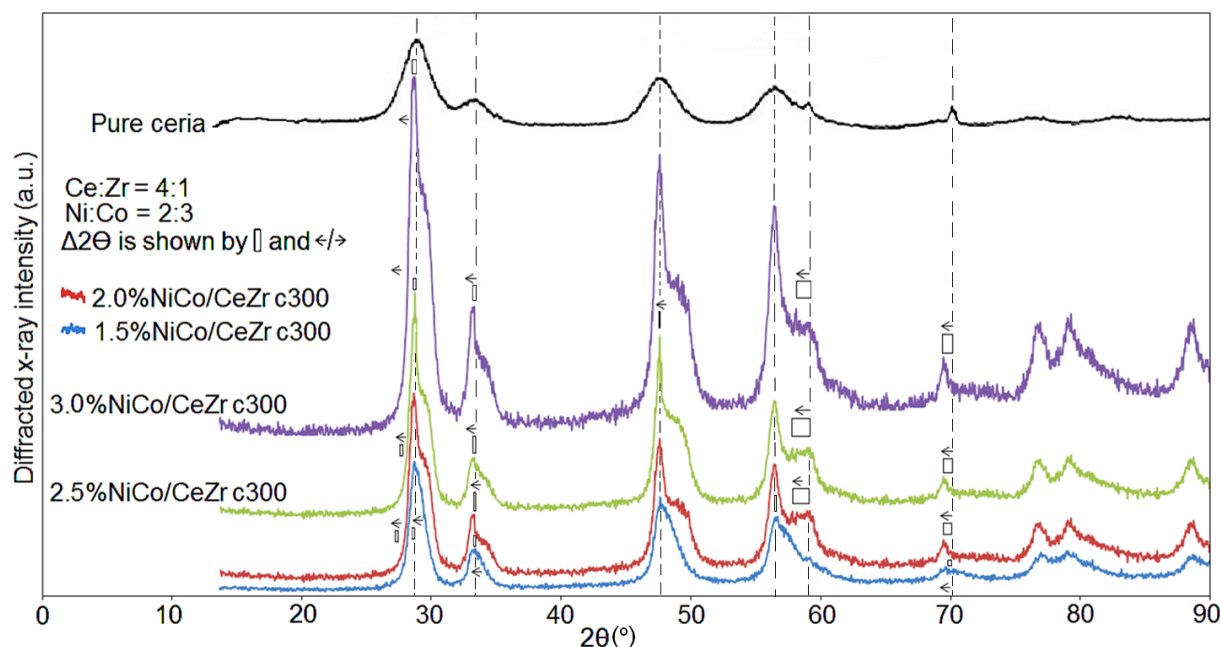


**Fig. S2** XRD diffractograms of 1.5 wt. % NiCo, 2.0 wt. % NiCo, 2.5 wt. % NiCo and 3.0 wt. % NiCo supported on CeZr mixed oxides support calcined at 300 °C, in comparison to pure ceria, with  $\Delta 2\theta$  displayed showing the shifting of the characteristics peaks from pure ceria.

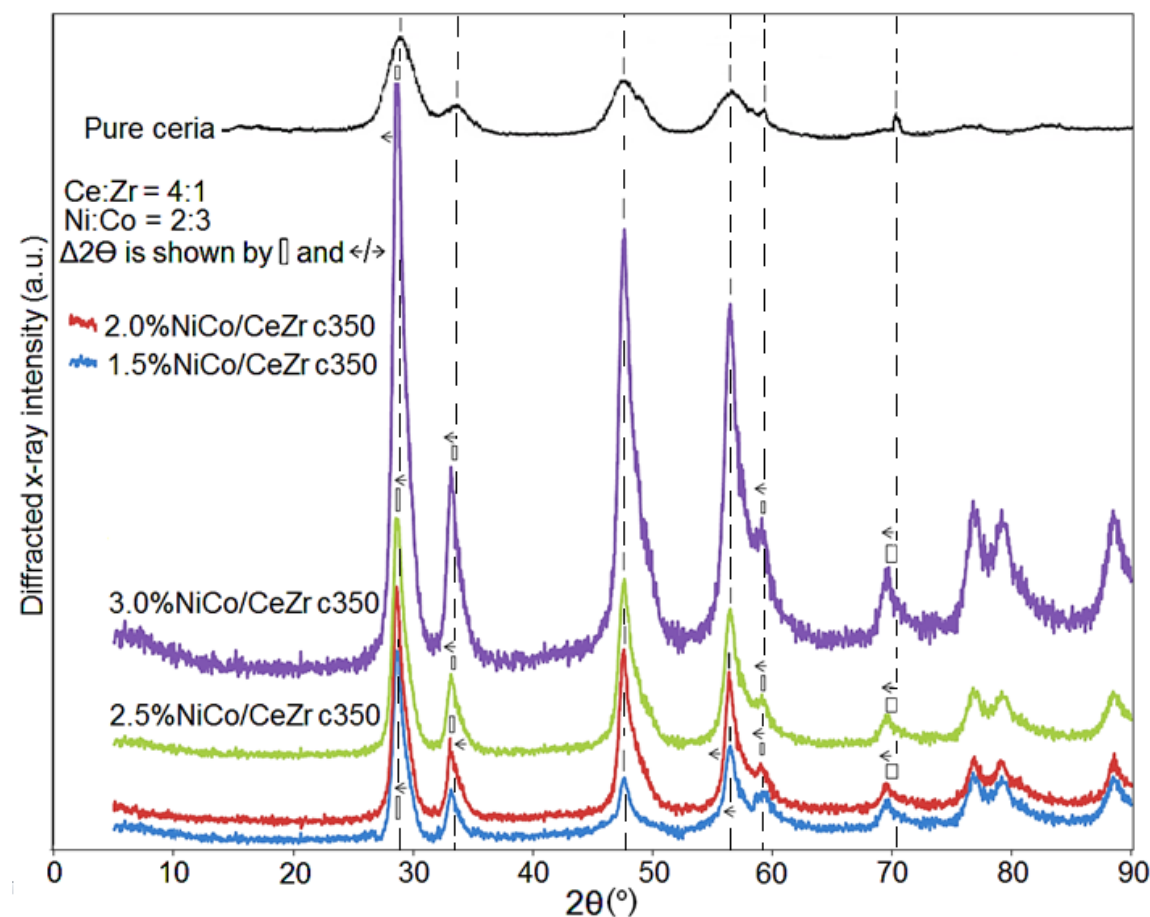


**Fig. S3** XRD diffractograms of 1.5 wt. % NiCo, 2.0 wt. % NiCo, 2.5 wt. % NiCo and 3.0 wt. % NiCo supported on CeZr mixed oxides support calcined at 350 °C, in comparison to pure ceria, with  $\Delta 2\theta$  displayed showing the shifting of the characteristics peaks from pure ceria.

## S.2.2 Pore size distribution of supported catalysts

Fig. S4 depicts the pore size distribution obtained from BJH desorption, showing pore volume as a function of pore diameter for: (a) CeZr support c300, c350, c400 (b) 1.5 to 3.0% NiCo/CeZr c300 catalysts (c) 1.5 to 3.0% NiCo/CeZr c350 catalysts (d) 1.5 to 3.0% NiCo/CeZr c400 catalysts, respectively. It can be seen that bimodal distribution exists for all CeZr supports in Fig. S4a, but only 3.0%NiCo/CeZr c300 catalyst in Fig. S4b, all catalysts in Fig.S4c except for 1.5%NiCo/CeZr c350 which is unimodal, and lastly, all catalysts in Fig. S4d except for 2.5%NiCo/CeZr c400 support (unimodal) and 3.0%NiCo/CeZr c400 (quadruple modal). This bimodal distribution characteristic is commonly found for conventional Zr materials that contain intra and inter-agglomerate pores derived from Zr-based solid solutions prepared by chemical techniques. Extremely narrow and sharp peak is detected for CeZr c350 support at 3.8 nm. Contrarily, a broader peak recorded at 9.4–10.4 nm was found for this support. Notably, it is beneficial to have bimodal pore size distribution over unimodal one, because whilst smaller pores offer larger surface areas to disperse active metallic particles more effectively, larger pores have their advantage per se, i.e. to increase mass transfer rate of biogas molecules onto the catalyst surface during MDR. Discussion is omitted for Fig. S4b since this result is the least promising of all graphs. In Fig. S4c, two sharp peaks were measured at 3.4-3.5 nm for 1.5 and 2.0%NiCo/CeZr c350, whereas two minor peaks were shown at the same range for 2.5 and 3.0%NiCo/CeZr c350. These small pores can be used to enhance the total MDR activity and stability by virtue of the creation of more defects and the containment of smaller particles.<sup>2</sup>

On the other hand, concerning MDR activity, it is postulated that diffusion limitation and the resistance to mass transfer can be decreased with pores that are slightly larger. These larger pores can be found in 2.5%NiCo/CeZr c350 (7.4 nm), 3.0%NiCo/CeZr c350 (11.2 nm) and 2.0%NiCo/CeZr c350 (13.6 nm) catalysts. Presumably, the dispersion of active phase solids on these supported catalysts will not be hindered at the same time. Similar phenomenon was perceived for all catalysts with 1.5 to 3.0 wt. % NiCo loading and their CeZr support calcined at 400 °C. However, in this case, the smaller pore size range was 3.3-3.7 nm, in which the very sharp, distinct peaks are assigned to 2.5 and 3.0%NiCo/CeZr c400 catalysts, and the smaller ones to 1.5 and 2.0%NiCo/CeZr c400 instead. With regard to the broader pore size distribution peaks, 3.0%NiCo/CeZr c400 contains slightly larger pore size ranging from 7.6 to 8.6 nm, and 11.2 nm; pore size of 10.1 nm for 2.0%NiCo/CeZr c400 and 13.5 nm for 1.5%NiCo/CeZr c400 solids were noted. Results are in accordance to pore size measured from N<sub>2</sub> sorption as shown in Table 1 (main article). The importance in distinguishing the pore size distribution curves resides in the fact that different bimodal catalysts yield different reaction rates due to varied diffusion efficiency, which was also previously discussed in the MDR activity section (Section 3.4 in the main article). It is also worthwhile to note that all the hysteresis loops of these BET analyses were of type IV ((Brunauer, Deming, Deming and Teller) BDDT classification),<sup>3</sup> characterized by adsorption and desorption branches nearly parallel to each other in a considerable range of P/P<sub>0</sub>. This in turn also happened to be often found in near-spherical agglomerated particles with uniform size and coordination number.

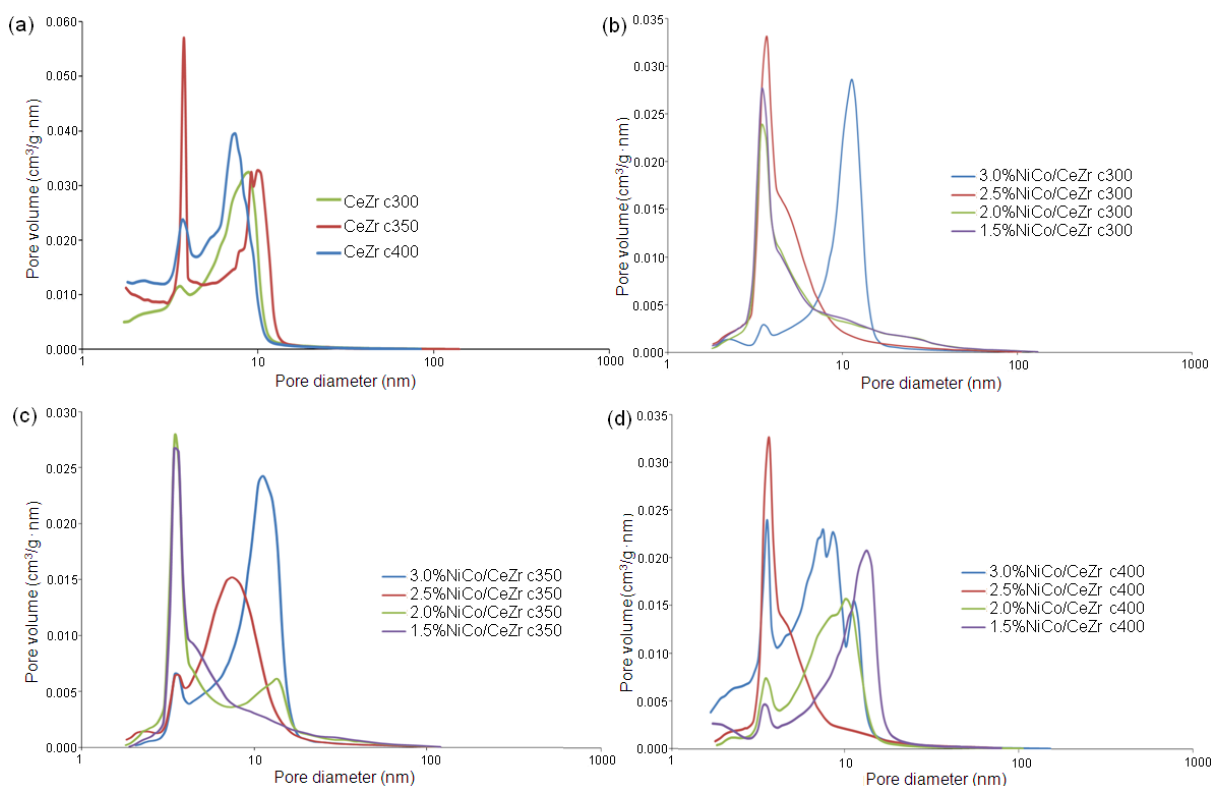


**Fig. S4** Pore size distribution obtained from BJH desorption, showing pore volume as a function of pore diameter for (a) CeZr support c300, c350, c400, (b) 1.5 to 3.0% NiCo/CeZr c300 catalysts, (c) 1.5 to 3.0% NiCo/CeZr c350 catalysts, and (d) 1.5 to 3.0% NiCo/CeZr c400 catalysts.

### S.2.3 Thermal analysis via TG-DSC techniques for supported catalysts

Fig. S5 displays the TG-DSC profiles of all as-synthesized catalysts, exhibiting their respective derivative weight curves as a function of temperature for (a) catalysts with varied NiCo loading quantity (1.5, 2.0, 2.5 and 3.0 wt. %) but CeZr supports calcined at 300 °C, (b) at 350 °C, (c) at 400 °C, respectively; (d) derivative heat flow as a function of temperature for catalysts with varied NiCo loading quantity (1.5, 2.0, 2.5 and 3.0 wt. %) but CeZr supports calcined at 300 °C, (e) at 350 °C, (f) at 400 °C, respectively. In Fig. S5a, only one peak was observed for 1.5%NiCo/CeZr c300 and 2.5%NiCo/CeZr c300, at 102.6 and 109.8 °C, respectively. For 2.0%NiCo/CeZr c300, two peaks were located, i.e. at 85.0 and 336.8 °C. On the other hand, for 3.0%NiCo/CeZr c300, three peaks were found, i.e. 100.3, 268.7 and 358.3 °C. All four peaks (one of each) from the four samples that revolve around 100 °C resulted from loss of adsorbed moisture.<sup>4</sup> They correspond to the derivative endothermic heat flow curves in Fig. S5d, which also fell within the same range. The exothermic peaks that appear at higher temperatures, for instance, 300 °C for 1.5%NiCo/CeZr c300 could be elucidated by the thermal effect on their phase transformation from amorphous to nanocrystallites, and on the other hand, 384 °C for 3.0%NiCo/CeZr c300 is attributed to the exothermic crystallization of Zr.

In Fig. S5b, aside from peaks arising between 70 and 300 °C contributed by the loss of non-dissociative water molecules and residual or existing hydroxyl groups, additional signals were identified in 2.5%NiCo/CeZr c350 at 460 and 568.3 °C. Beyond 600 °C, the derivative heat flow curves as shown in Fig. S5d-f for 1.5%, 2.0%NiCo/CeZr c300 and all of NiCo catalysts for CeZr c350, alongside 1.5%NiCo/CeZr c400 altogether indicate the decomposition of remaining nitrate groups originated from the support and catalyst precursors.<sup>5</sup> As a matter of fact, the weight losses above 250 °C (as shown in Fig. S5b for 2.5%NiCo/CeZr c350 at 257 °C, Fig. S5c for 1.5%NiCo/CeZr c400 at 267 °C, 2.0%NiCo/CeZr c400 at 296 °C, 2.5%NiCo/CeZr c400 at 308 °C) is ascribed to the decomposition of Ce and Zr nitrates and the removal of glycol, organic acid or ester compounds

originated from part of applied catalyst synthesis procedure, which involved sample mixing and hydrothermal autoclaving. From Fig. S5a–c, one can also detect no further weight loss change exceeding 500 °C, proving that the selection of calcination temperature range for our work is suited for a mono-phasic  $\text{Ce}_{1-x}\text{Zr}_x\text{O}_2$  nanocrystallites support. In Fig. S5e, a discernible shoulder can be seen for all 1.5% to 3.0%NiCo/CeZr c350 catalysts at the onset of their second endothermic peak at around 200–250 °C, due to the release of nitrates precursors, which is in line with the derivative weight curves.<sup>6</sup>

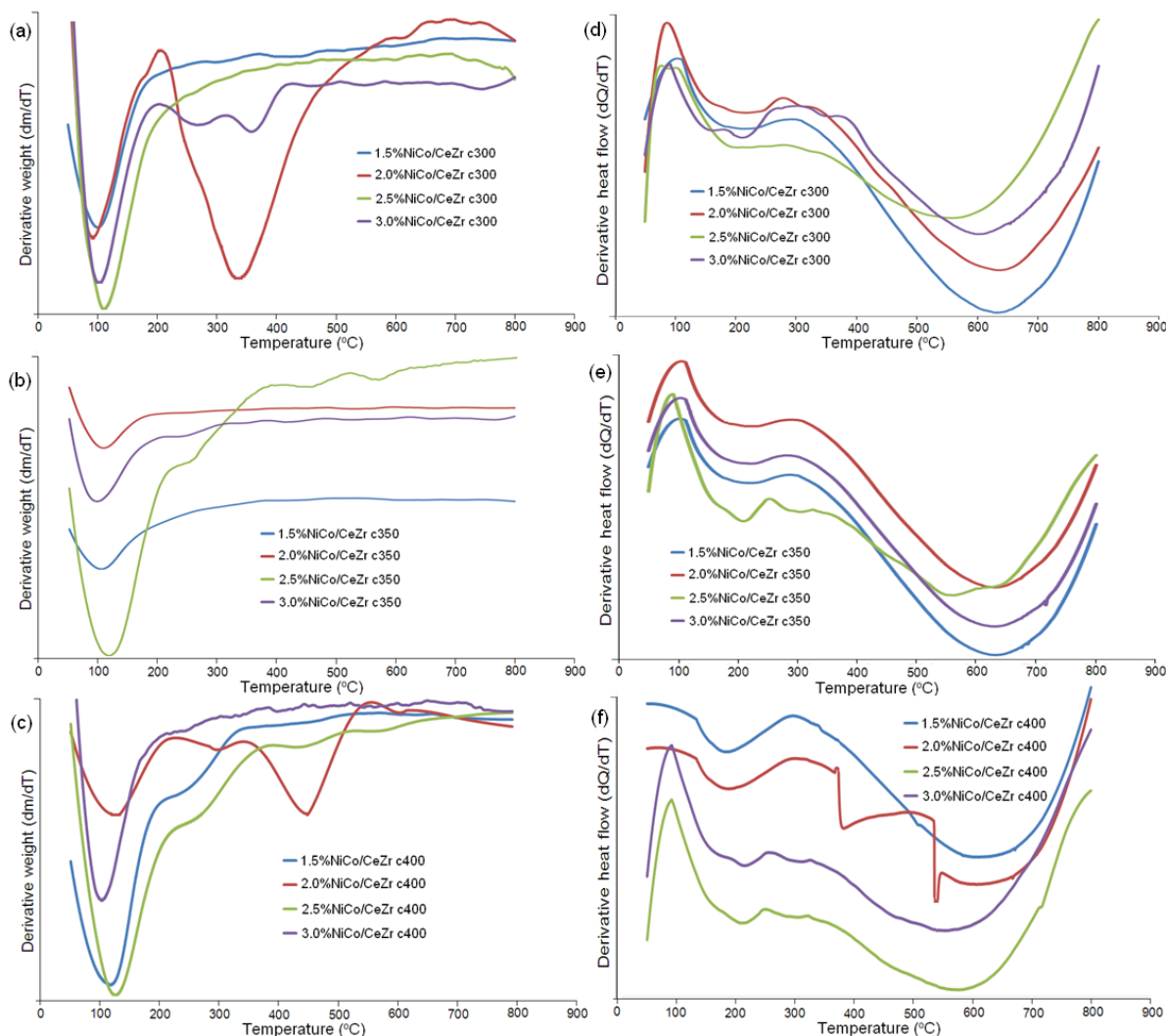


**Fig. S5** TG-DSC profiles with derivative weight as a function of temperature for (a) catalyst with varied NiCo loading quantity (1.5, 2.0, 2.5 and 3.0 wt. %) but CeZr support all calcined at 300 °C, (b) at 350 °C, (c) at 400 °C; (d) derivative heat flow as a function of temperature for catalyst with varied NiCo loading quantity (1.5, 2.0, 2.5 and 3.0 wt. %) but CeZr support all calcined at 300 °C, (e) at 350 °C, (f) at 400 °C.

**S.2.4 MDR activity tests for 20 h time on stream: Biogas conversion and syngas production**

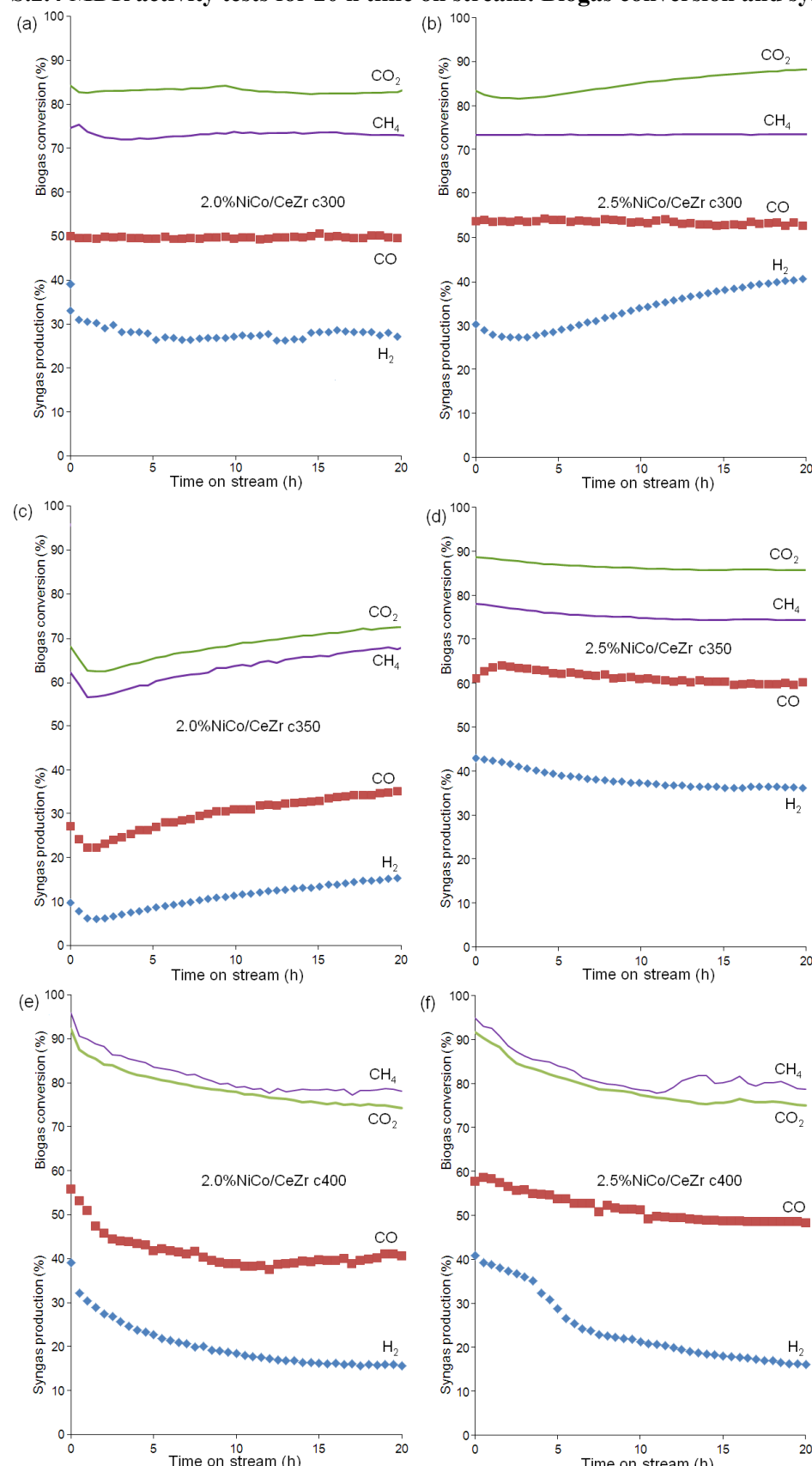


**Fig. S6** Syngas production and biogas conversion profiles after 20 h MDR reaction for (a) 2.0%NiCo/CeZr c300, (b) 2.5%NiCo/CeZr c300, (c) 2.0%NiCo/CeZr c350, (d) 2.5%NiCo/CeZr c350, (e) 2.0%NiCo/CeZr c400, and (f) 2.5%NiCo/CeZr c400 catalysts.

## References

- 1 D. A. M. Monti and A. Baiker, *J. Catal.* 1983, **83**, 323.
- 2 E. L. G. Oliveira, C. A. Grande and A. Rodrigues, *Fuel Process. Technol.*, 2010, **65**, 1539.
- 3 K. S. Sing, D. H. Everett, R. A. W. Haul, L. Moscou, R. A. Pierotti, J. Rouquerol and T. Siemieniewska, *Pure Appl. Chem.*, 1985, **57**, 603.
- 4 B. M. Reddy, P. Lakshmanan and A. Khan, *J. Phys. Chem. B*, 2005, **109**, 13545.
- 5 L. Liu, Z. Yao, B. Liu and L. Dong, *J. Catal.*, 2010, **275**, 45.
- 6 H. Li, L. Zhang, H. Dai and H. He, *Inorg. Chem.*, 2009, **48**, 4421.